Materials & Design 224 (2022) 111358

Contents lists available at ScienceDirect

Materials & Design

journal homepage: www.elsevier.com/locate/matdes

Automation of intercept method for grain size measurement: A topological skeleton approach

Xiang Li [a], Linyi Cui [c], Jikang Li [b], Ying Chen [b], Wei Han [b], Sara Shonkwiler [a], Sara McMains [a,*]

[a] University of California, Berkeley, United States
[b] China Iron and Steel Research Institute Group, China
[c] The Hong Kong Polytechnic University, Hong Kong, China

HIGHLIGHTS

- A novel algorithm to automate the intercept method for grain size measurement.
- Identifying and classifying intersections in accordance with international standards.
- Significantly reducing measurement error and time compared to commercial software.

GRAPHICAL ABSTRACT

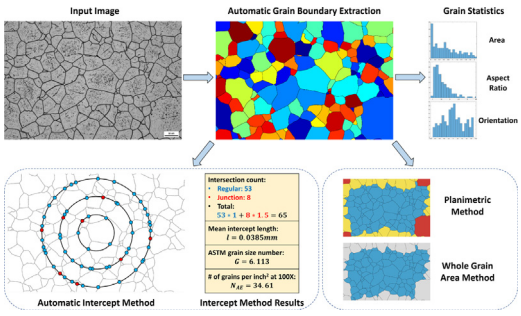

ARTICLE INFO

Article history:
Received 23 June 2022
Revised 4 November 2022
Accepted 8 November 2022
Available online 10 November 2022

Keywords:
Grain size measurement
Intercept method
Microstructure characterization
Topological skeleton
Image analysis

ABSTRACT

In the microstructure characterization of metallic materials, the intercept method is one of the most widely accepted approaches to determine average grain size due to its simplicity, accuracy, and the ability to handle both equiaxed and non-equiaxed grain structures. However, its manual implementation is relatively time-consuming and error-prone, and the design of automated implementations is challenging due to the requirement of recognizing, classifying, and scoring different types of intersections (between test patterns and grain boundaries) by international standards such as ASTM E112 and EN ISO 643. In this research, a novel algorithm is proposed to automate the intercept method for grain size measurement from microscopic images. Building on topological skeletons, the algorithm is able to extract continuous and closed grain boundaries from the raw image, and determine the average grain size by recognizing and classifying different types of intersections in accordance with international standards. The effectiveness and efficiency of the proposed algorithm is validated on metallographic microscope images from both high-purity iron and stainless steel. Additionally, our algorithm has been extended to automate other standard grain size measurement methods such as the planimetric method and the whole grain area method.

1. Introduction

Grain size measurement from microscope images is an important task for the microstructure characterization of metallic materials. The internal structures of metallic materials are made up of individual crystalline areas possessing their own distinct orientations, which are known as grains. The average grain size of the metallic materials has significant influence on their mechanical and material properties such as strength [1,2], corrosion behavior [3], hot deformation behavior [4], and fracture behavior [5]. An accurate measurement of the average grain size enables

* Corresponding author.
E-mail address: mcmains@berkeley.edu (S. McMains).

https://doi.org/10.1016/j.matdes.2022.111358
0264-1275/

researchers to understand material microstructures, predict material properties/behaviors, and optimize manufacturing parameters [6].

Grains can be observed from cross-sectional microscope images of metallographic specimens after a series of preparation steps such as polishing and etching. Because of the importance and effectiveness of grain size measurement for material microstructure characterization, official standards for determining average grain size from microscope images are published and regulated across countries, such as ASTM E112 [7] (United States), EN ISO 643 [8] (Europe/International), JIS G 0551 [9] (Japan), and GB/T 6394 [10] (China). In these standards, three traditional micrographic methods are described to determine the average grain size: the comparison method, the planimetric method, and the intercept method. These standard test methods are usually performed manually, which makes the measurement process time-consuming and error-prone.

Image processing techniques are widely used in microstructure characterization of various materials for increased efficiency and accuracy [11–15]. To measure the average grain size of metallic materials, various automatic or semi-automatic image processing algorithms have been developed. Based on connectivity and morphological operations, Peregrina-Barreto et al. [16] proposed automatic image thresholding and segmentation processes to identify individual grain regions. By utilizing the concept of ultimate opening and top-hat transformation, Paredes-Orta et al. [17] developed a watershed-segmentation-based algorithm to separate individual grains. Banerjee et al. [18] applied Canny edge detection and an elaborate region-expansion process to determine grain sizes of interstitial-free steels. Building on MATLAB image processing tools, García-García et al. [19] proposed a semi-automatic approach to characterize grain size distribution of austenitic steels. Flipon et al. [20] designed an semi-automatic image analysis procedure to extract grain boundaries by utilizing edge detection and watershed segmentation algorithms.

Most of these existing approaches focus on procedures to preprocess input images and identify individual grain areas (or similarly, extract grain boundaries). After individual grain identification, these approaches generally employed the planimetric method [7] to determine the average grain size because its calculation process is straightforward under computer-aided operations. The average grain size can be conveniently calculated by the planimetric method from locations and sizes of identified grain areas (see Section 3.5.2 for details). However, the planimetric method's effectiveness is limited to uniformly equiaxed grains (whose axes have approximately the same length).

The intercept method is one of the most widely accepted micrographic methods due to its simplicity, accuracy, and applicability to both equiaxed and non-equiaxed grain structures. Thus, in the official standards, the intercept method is the preferred test method recommended for evaluating materials with all forms of grain structures, no matter if they are uniformly equiaxed or not [7–10]. Banerjee et al. [18] and Flipon et al. [20] discussed the use of the intercept method in their grain size measurement algorithms, but did not provide an automatic solution in compliance with the standards, in particular identifying special types of intersection points located at particular positions such as grain junctions (which should be scored as multiple intersections according to the standards). The largest challenge to automate the intercept procedure is to automatically identify and classify these special types of intersections in accordance with the standards (see Section 2.2 for more details).

An alternative approach to determine average grain size is to develop predictive models using machine learning techniques [21,22]. The accuracy of machine learning models largely depends on the amount of high-quality labeled data. Since manual labeling processes are usually less efficient and consistent, automatic image processing algorithms for determining and labeling grain sizes would further improve the effectiveness of machine-learning-based approaches.

Therefore, in this paper, we propose a novel automatic algorithm to determine grain sizes of metallic materials (Fig. 1) based on the intercept method because of its wide applicability and acceptance by industry. By exploiting topological skeletons [23], our approach is able to follow the intercept procedure as it is specified by the standards [7–10], recognizing and scoring all the different types of intersection points that were not handled by previous work. This includes junction intersection points, the most challenging to automate. Additionally, our algorithm could be easily extended to automate other standard grain size measurement methods such as the planimetric method [7–10] and the whole grain area method [24]. Our implementation is useful not only to automatically determine average grain size for material microstructural characterization, but also as an educational tool for improving students' and researchers' understanding of the procedure details of standard grain size measurement methods by generating and visualizing real-world measurement examples. The efficiency and effectiveness of our algorithm are validated on real-world microscopic images of both high-purity iron and stainless steel.

2. Materials and methods

In this section, we first describe the materials and microscope images being used for developing and testing our algorithm (Section 2.1). We then provide background on the intercept method and its differences across the standards (Section 2.2). Finally, we introduce our automatic grain size measurement algorithm and provide implementation details (Section 2.3).

2.1. Materials and microscope images

In order to test the robustness and generality of our algorithm on characterizing microstructures of different materials, we prepared a total of 200 microscope images generated from high-purity iron and stainless steel specimens (100 images from each material, see Fig. 2 for example inputs). The ASTM grain size numbers [7] of these specimens range from 3 to 7.

Our specimens were prepared in accordance with ASTM E3-11 "Standard Guide for Preparation of Metallographic Specimens" [25]. The microscopy and specimen preparation specifications are listed in Table 1.

As a consequence of different material microstructures and etching methods, microscope images generated from high-purity iron and stainless steel have dissimilar characteristics. For example, compared to microscope images of high-purity iron, images of stainless steel have a higher contrast between grains and grain boundaries. However, they also experience higher noise and impurity levels (Fig. 2).

Therefore, these two classes of microscope images help us test and improve the applicability of our algorithm on microscope images of different materials, under different image and specimen preparation conditions.

2.2. The intercept method

Official standards [7–10] provide and specify the intercept method as one of the standard test methods for determining average grain size. It is the only one of these standard test methods recommended for measuring the average grain size of both uniformly equiaxed grain structures and anisotropic grain structures.

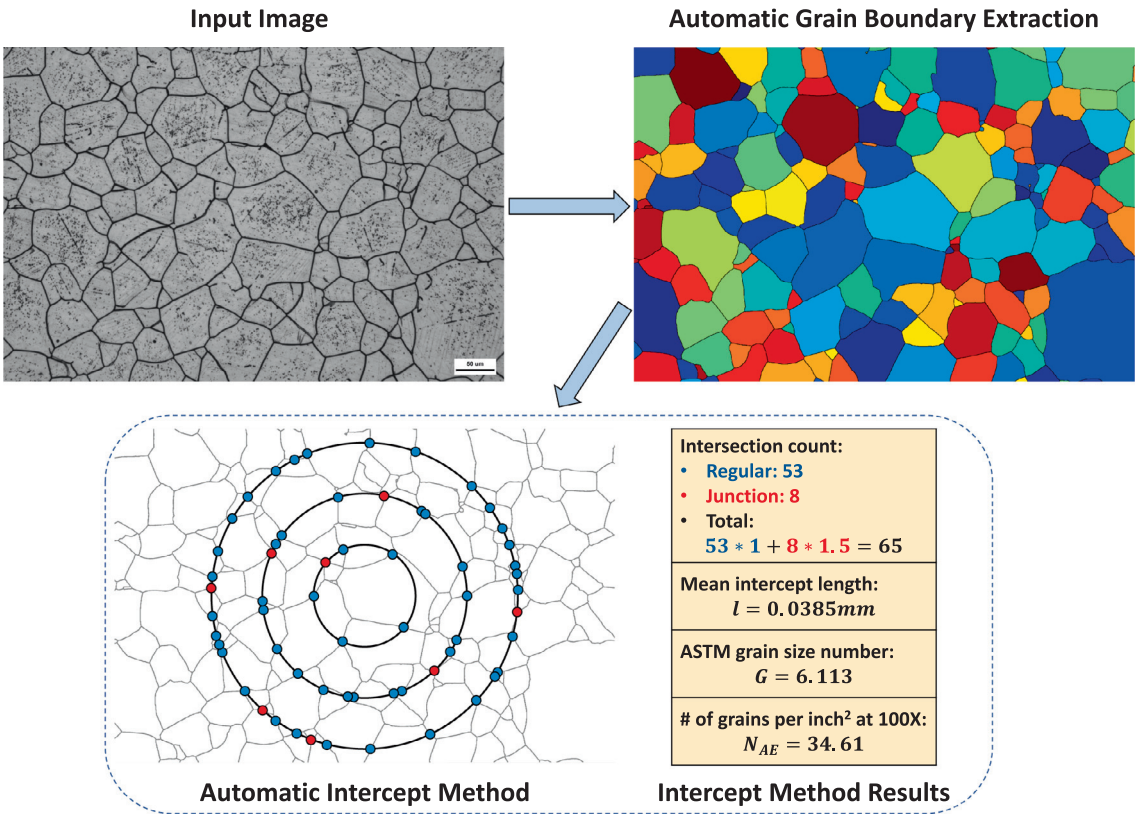

Fig. 1. An example input image (and test pattern) showing the experimental results of our algorithm to measure grain size by automating the intercept method.

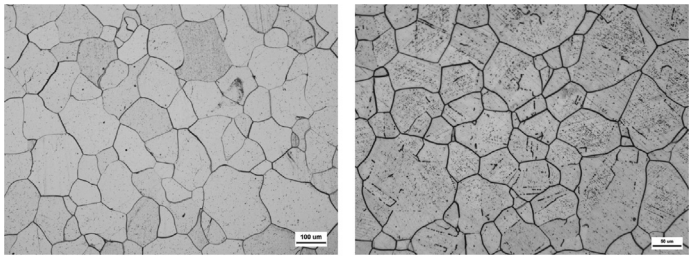

Fig. 2. Examples of input microscope images with the two types of microstructures: (a) ferrite grains from high-purity iron; (b) austenite grains from stainless steel.

Table 1
Details of the metallographic preparation procedure.

	High-purity iron	Stainless steel
Microstructure	Ferrite	Austenite
Cutting	Metallographic cutting machine	
Grinding	1000-grit sandpaper	
Polishing	Polishing cloth	
Etching	Nital	1 g $KMnO_4$ +10 ml H_2SO_4 +90 ml H_2O
Microscopy	Leica DMi8C microscope; magnification: 100x or 200x; image size: 5472*3648 pixels	

The main idea of the intercept method is to draw random test patterns (lines or circles) on microscope images, and count the number of intersections ($N_{intersections}$) between test patterns and grain boundaries. The number of grains per square inch at 100X magnification (denoted as N_{AE}) and the grain size number (denoted as G, a widely used grain size evaluation index) can be then calculated from the number of intersections by the following equations [7–10]:

$$N_{AE} = 2^{G-1} \tag{1}$$

$$G = -3.288 - 6.643856 * \log_{10}\ell \tag{2}$$

where ℓ is the mean intercept length (in mm) that can be calculated from:

$$\ell = \frac{L}{M * N_{intersections}} \tag{3}$$

where L is the total length of test patterns (in mm), M is the magnification of the microscope, and $N_{intersections}$ is the number of intersections. Since L and M are generally constant during the evaluation of the same batch of microscope images, correctly counting the number of intersections ($N_{intersections}$) is the most critical task in the intercept method.

Fig. 3 shows real-world examples of two commonly used intercept methods and their test patterns: the so-called "lineal" intercept procedure [26] that employs straight test lines, and the circular intercept procedure [27,28] that employs one or multiple (concentric) test circles.

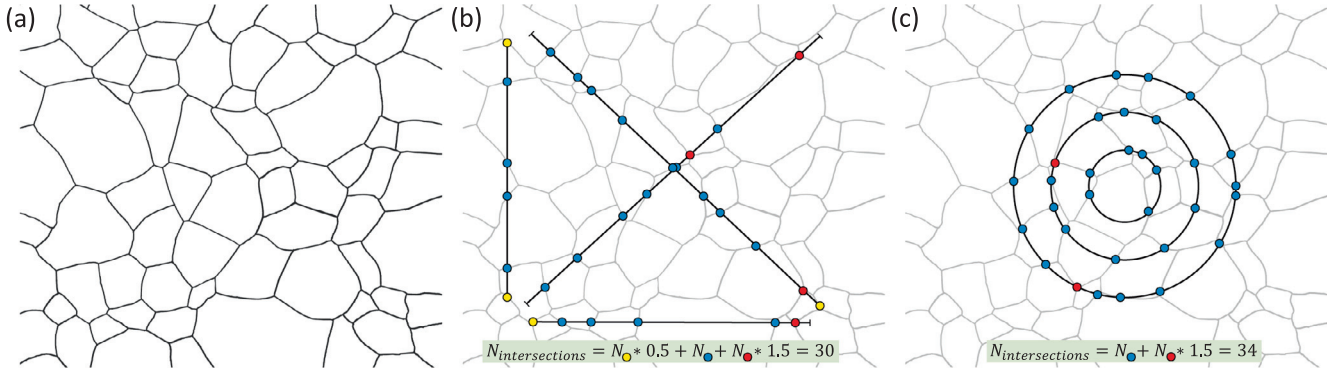

Fig. 3. Examples of two common intercept patterns: (a) a real-world example of grain structure (after applying our grain boundary extraction procedure), (b) Heyn lineal intercept procedure [26], (c) Abrams three-circle procedure [27]. Red points represent junction intersections that should be scored as 1.5 intersections; yellow points represent test line end point intersections that should be scored as 0.5 intersections; blue points represent all other "regular" intersections [7].

The international standards [7–10] provide following rules for the intersection counting process:

- Intersections at the junction points of three grains should be scored as 1.5 or 2 (see Fig. 3 red intersection points).
  - For lineal intercept procedures, junction intersections should be scored as 1.5.
  - For circular intercept procedures, junction intersections should be scored as 1.5 following ASTM E112 (United States) [7]; or be scored as 2 following EN ISO 643 (Europe) [8], JIS G 0551 (Japan) [9], or GB/T 6394 (China) [10] standards.
- Intersections at ends of test lines should be scored as 0.5 (only applicable for the lineal intercept procedure; see Fig. 3 yellow intersection points).
- All other intersections should be scored as 1.

In this research, we design an algorithm to automate the intercept procedure that is able to identify and classify the intersections into the aforementioned scoring types in accordance with the standards. Although all the standards could be handled by our algorithm, for the ease of demonstration, we adapt the ASTM standard [7] and score all the junction intersections as 1.5 in examples throughout this paper.

2.3. Algorithm details

In shape analysis, the topological skeleton refers to a thin version (usually one-pixel wide) of the input shape, where all pixels of this resulting skeleton are equidistant from the boundary of the input shape.

Exploiting topological skeletons, we design an algorithm that automates the intercept method for grain size measurement from microscope images (Fig. 4). In the algorithm, we first pre-process input images, segmenting them into potential grain and grain boundary regions by adaptive thresholding (Section 2.3.1). Then, we extract grain boundaries and identify individual grains by constructing and analyzing topological skeletons of the thresholded grain boundary regions/pixels (Section 2.3.2). Finally, by utilizing grain junction points identified from the topological skeleton, we compute intersections between test patterns and grain boundaries, classify them into the different intersection types, and calculate average grain sizes and grain size numbers (Section 2.3.3).

The topological skeleton enables us to extract grain boundaries, separate individual grains, and identify intersection points accurately and robustly. This approach's advantages include:

- preserving the connectivity information of grain boundaries,
- eliminating the interference from variations of grain boundary thickness,
- reducing the sensitivity to image noise and microstructural artifacts adjacent to grain boundaries,
- recognizing partially missing/broken grain boundaries and assisting in completing/connecting them, and
- identifying grain junctions for intersection classification (in order to implement the intercept method).

2.3.1. Pre-processing and image thresholding

Starting with the input microscope image (Fig. 4(a)), our algorithm first converts it to grayscale and removes high-frequency image noise by applying Gaussian smoothing. In these grayscale images, grain boundary pixels are visually darker than the grain pixels and can generally be segmented by global thresholding techniques such as Otsu's method [29]. However, global thresholding techniques perform less efficiently on poor-quality images (e.g. under uneven lighting conditions), which are not rare in microscopic images of metallic materials [17].

Adaptive thresholding [30] is designed to handle both good and poor quality images by first estimating their background illumination conditions, and then implementing local thresholding operations accordingly (see an example in Fig. 5). Therefore, we apply the adaptive thresholding method in our algorithm for effective grain and grain boundary pixel segmentation (Fig. 4(b)) from images of various qualities.

After adaptive thresholding, we obtain a binary image representing our preliminary segmentation of grain and grain boundary pixels. To further clean this binary image, we utilize morphological opening and area opening operations [31] to remove isolated image noise and microstructural artifacts (e.g. small holes, scratches, or stains).

2.3.2. Grain boundary extraction

After segmenting the original image into grain and grain boundary pixels, we construct a topological skeleton of the grain boundary using the algorithm of Lee et al. [23]. In the topological skeleton, grain boundaries appear as long, connected edges, whereas noise/artifacts attached to grain boundaries tend to appear as short dangling branches (Fig. 6), and discontinuous grain boundaries appear as long dangling branches (Fig. 7).

In our algorithm, users have the choice to define the threshold to distinguish long and short dangling branches, which correspond to discontinuous boundaries and noise/artifacts respectively, as a percentage of the average length of skeleton edges (grain bound-

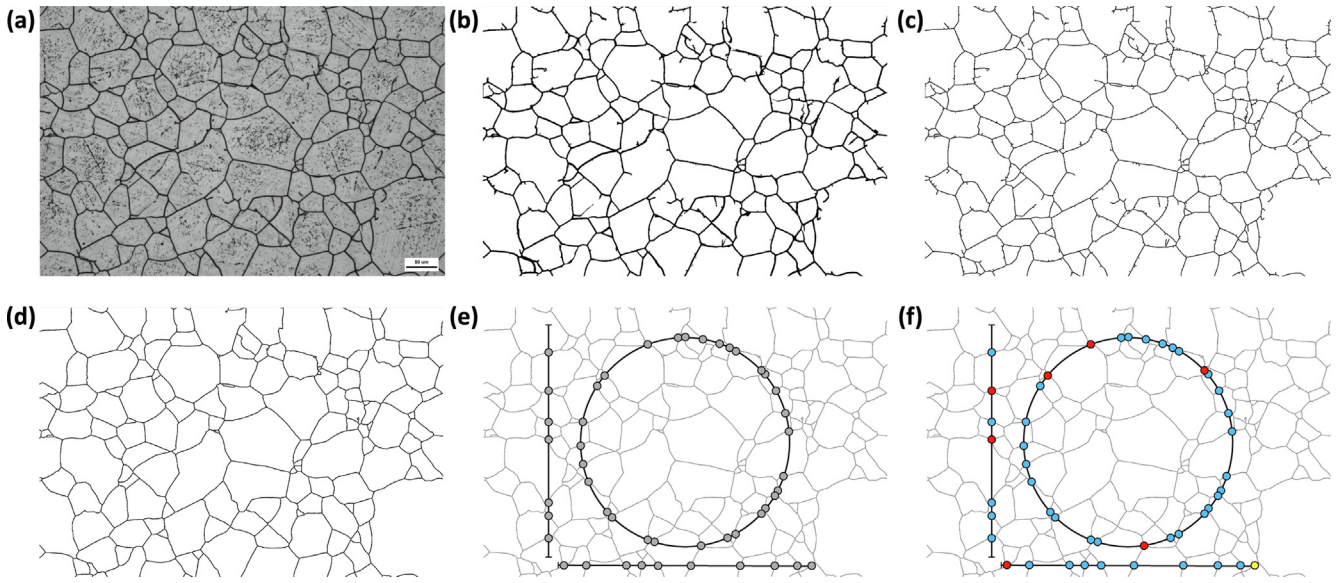

Fig. 4. Full algorithm overview: (a) input image, (b) adaptive thresholding results, (c) skeletonization, (d) skeleton/branch pruning, (e) intersection computation, (f) intersection classification. Step (b-d) are designed to extract continuous and closed grain boundaries; and step (e,f) are designed to correctly count intersections in accordance with the standards.

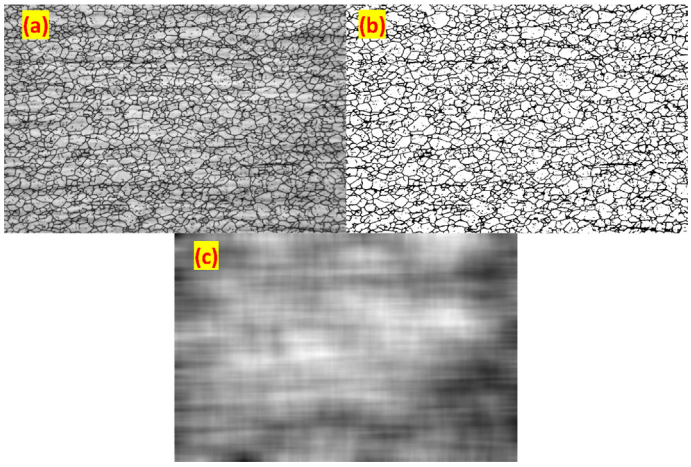

Fig. 5. An example of adaptive thresholding on images under uneven lighting conditions: (a) input image, (b) thresholding result, (c) estimated background illumination.

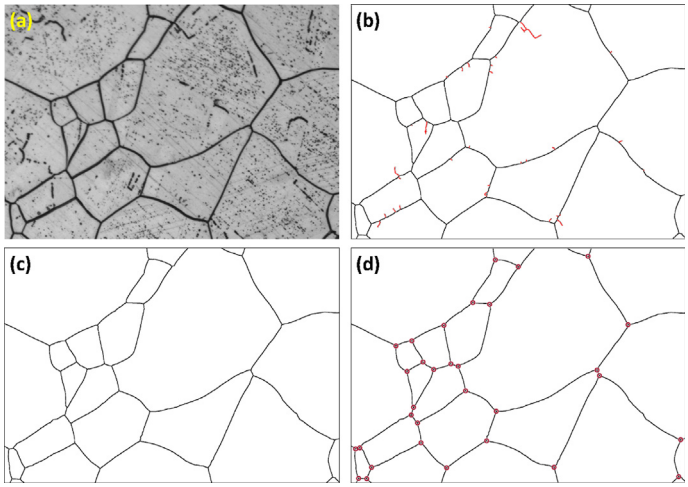

Fig. 6. An example of the grain boundary extraction and junction point identification process: (a) input image, (b) the topological skeleton (branches in red), (c) resulting grain boundaries after pruning branches from the skeleton, (d) identified grain junction points (in crimson).

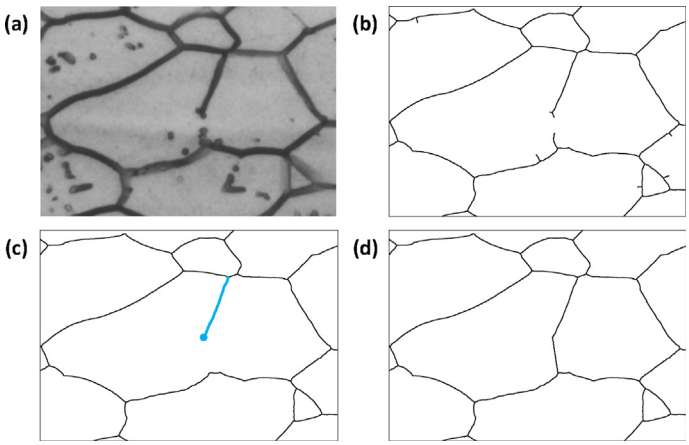

Fig. 7. An example of discontinuous grain boundary completion/connection: (a) input image; (b) the topological skeleton; (c) grain boundaries after pruning short branches, with the discontinuous grain boundary and its free end highlighted in blue; (d) resulting grain boundaries after completing/connecting the discontinuous boundary.

aries). Our experiments show that setting this threshold length as 50% of the average length of skeleton edges generally provides good results for our dataset.

Thus, the topological skeleton allows us to distinguish (with high accuracy) such noise and artifacts from true grain boundaries, allowing us to prune short dangling branches from the skeleton. Note that the pruning of original branches may cause the generation of new dangling branches. Therefore, we iteratively implement the branch pruning process until no more short dangling branches exist (Fig. 6(c)). During the construction of the skeleton, the junction points among individual grains are also identified (Fig. 6(d)). These junction points will be utilized to recognize junction intersections, as required for the intercept method (see Section 2.3.3).

As shown in Fig. 7, after the pruning of short branches, discontinuous grain boundaries may (and are likely to) still exist in real-world microscope images depending on various factors such as the characteristic of the material, the quality of the specimen preparation process, and/or the illumination conditions during the micro-imaging process. In the topological skeleton, discontinuous grain boundaries are represented as long dangling branches.

During the iterative branch pruning process, we retain these long dangling branches, and provide three options for users to handle discontinuous grain boundaries:

1. Extend branches from their free ends until colliding with other edges.
2. Manually complete/connect branches.
3. Preserve discontinuous branches without completing/connecting them.

A comparison of the effectiveness of these three options is summarized in Table 2. On our real-world test images, where few grain boundaries are discontinuous, all of these three options work well with the intercept method and obtain similar grain size measurement results. Option 1 (extension) is recommended in general because it is fully automatic, and is able to identify/separate individual grains. Although individual grain separation is not necessary for the intercept method, it could help researchers conduct further microstructural analysis beyond the calculation of average grain sizes (see Section 3.5). With regard to applications that require high measurement accuracy, or when most of the grain boundaries are discontinuous, option 2 (manual connection) is recommended. Our implementation accelerates the manual branch completion/-connection process by highlighting long dangling branches and their free ends that need to be manually connected (Fig. 7(c)).

Table 2
Evaluation of different options for handling discontinuous grain boundaries (long dangling branches).

	Option 1 (Extension)	Option 2 (Manual Connection)	Option 3 (Preservation)
Accuracy	Good	Very Good	Good
Efficiency	Good	Fair	Good
Individual Grain Separation	Yes	Yes	No

After converting grain boundary pixels to a topological skeleton, pruning its short branches and connecting long branches, our algorithm extracts closed and continuous grain boundaries as well as their corresponding individual grains (Fig. 4(d)). Grain junction points are also identified for classifying regular/junction intersections in the intercept procedure (see Section 2.3.3).

2.3.3. Intersection recognizing and counting

In this step, the user is able to customize test patterns (a combination of test lines and/or concentric test circles) for the intercept procedure. With the test patterns, our algorithm first computes their intersections with identified grain boundaries (Fig. 4(e)). For the purposes of determining if an intersection has occurred, we need to take into consideration the original thickness of grain boundaries. We implement this tolerance ϵ as a thickness offset to be added on the grain junction points computed from the one-pixel-wide topological skeleton (where the effect of boundary thickness is eliminated). For an intersection, if its distance to any grain junction/end point is smaller than the user-defined offset parameter ϵ, our algorithm considers this intersection as being located at the corresponding junction/end point. In our experiments, we found that setting ϵ as the average grain boundary width (which can be easily obtained during the construction of the topological skeleton [23]) generally provided good measurement results (Fig. 8).

Then we classify these intersections as one of the three different types according to their relative locations with respect to test patterns and grain junction points:

1. If an intersection is within ϵ of any of the grain junction points, the intersection would be substituted by its corresponding grain junction point as a junction intersection in our algorithm. A junction intersection is scored as 1.5 in the intercept method

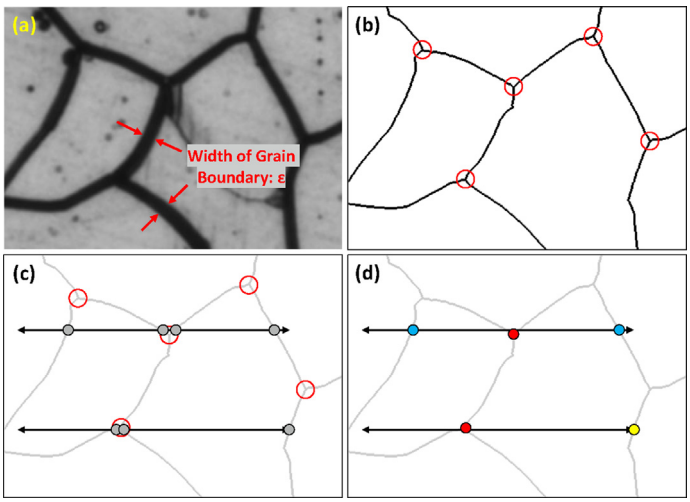

Fig. 8. An example of intersection recognition and classification in our automated intercept procedure: (a) an input image with average grain boundary width ϵ; (b) its topological skeletonization, and regions that count as grain junctions (in red circles with radii ϵ); (c) recognized intersections between two test lines and the topological skeleton; (d) classified intersections: regular intersections in blue, (test line) end intersections in yellow, and junction intersections in red. Multiple intersections close to the same grain junction are merged into a single junction intersection.

according to the ASTM standard [7]. Note if multiple intersections are close to the same grain junction point, such a grain junction point would only be counted as a junction intersection once (Fig. 8).
2. If an intersection is not located at a grain junction points, but is within ϵ of any of the test line ends, it would be determined as an end intersection by our algorithm and be scored as 0.5 in the intercept method.
3. If an intersection is neither a junction intersection nor an end intersection, it is a "regular" intersection and should be scored as 1 in the intercept method.

After computing and classifying the intersections (Fig. 4(f)), as the result of our automatic intercept procedure, our algorithm counts the total intersection scores, and calculates the average grain size as well as the ASTM grain size number by applying Eqs. (1)–(3).

3. Results and discussion

3.1. Overview

Our method successfully automates the intercept method for grain size measurement of all the 200 test microscope images, no matter if they are ferrite grains of high-purity iron or austenite grains of stainless steel. To evaluate the performance of our method, we also measure the average grain size of these microscope images both manually and using commercial software for comparison (Fig. 9). For all tests, the placement and shape (linear, circular, etc.) of test patterns was chosen randomly and preset for each image.

For the manual grain size measurement, three metallographic experts were invited to apply the intercept method (as described in ASTM E112 [7]) to manually determine the average grain size for each microscope images. Then anywhere the results differed, the experts corrected obvious oversights and then discussed remaining areas of disagreement (in either the existence or classification of intersections). They were eventually able to come to unanimous consensus, so grain sizes for all 200 images were used as ground truth results (see examples in Fig. 9(a,d)).

For the grain size measurement implementation using commercial software, a different three material experts, who were familiar with computer-aided image processing and metallographic software, were invited to apply the intercept method to determine the average grain size of our microscope images by selecting and applying appropriate commercial software. The experts suggested and implemented a semi-automatic procedure that first manually removes image noise and extracts grain boundary pixels using the image processing software provided by the microscope manufacturer Leica Microsystems [32], and then utilizes commercial metallographic software iCALIBUR Master [33] to automatically implement the intercept method on the extracted grain boundary pixels (see examples in Fig. 9(c,f)). Unfortunately, for this second step, to our knowledge no commercial software is able to classify intersections into the different intersection types and count them accordingly as described in the standards, so iCALIBUR Master actually only implements an approximation of the intercept method.

As shown in Fig. 9, to measure the average grain size of metallic materials by the intercept method, our proposed algorithm achieves basically the same level of accuracy as manual labeling, while significantly reducing the operation time, by 95%. Compared to the semi-automatic approach by commercial software that only recognizes intersection points, our automatic method is able to further classify and count them in accordance with the standards [7–10], which leads to better grain size measurement performance.

Next, we present detailed analysis of the accuracy and efficiency of our approach.

3.2. Accuracy

Five metrics are selected in order to evaluate and compare the accuracy of our approach and the semi-automatic commercial software approach (with the manual method as ground truth):

(a) **Precision of intersection recognition:**

$$Precision = \frac{\#\text{ of correctly recognized intersections}}{\#\text{ of recognized intersections}}. \quad (4)$$

The metric *Precision (Recognition)* answers the question: how many recognized intersections (by our approach or commercial software) are true/real intersections? This metric focuses on the intersection recognition process, and provides insight into the algorithm's ability to not generate false positives.

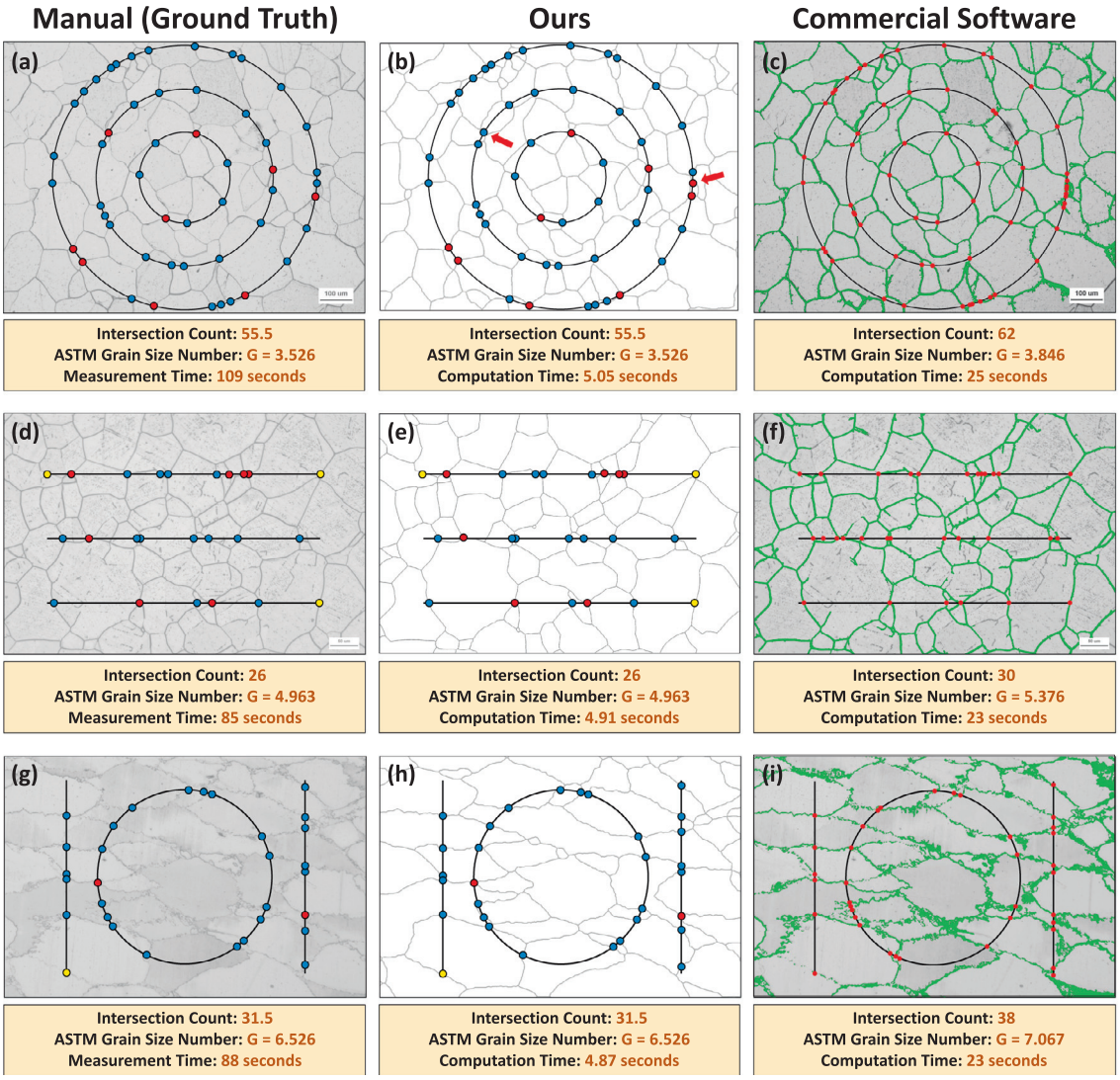

Fig. 9. Experimental result comparing grain size measurement using the intercept method as implemented by: manual labeling, our approach, and commercial software [32,33]. Upper row: results from an example image of equiaxed ferrite grain microstructure (high-purity iron); middle row: results from an example image of equiaxed austenite grain microstructure (stainless steel); lower row: results from an example image of elongated/non-equiaxed austenite grain microstructure (stainless steel). For the measurement of all types of grain structures, our method not only recognizes and classifies intersections in strict accordance with the standards [7–10], but also outperforms the commercial software in both accuracy and efficiency.

(b) **Recall of intersection recognition:**

$$Recall = \frac{\#\text{ of correctly recognized intersections}}{\#\text{ of true intersections}}. \tag{5}$$

The metric *Recall (Recognition)* answers the question: how many true intersections are correctly recognized (by our approach or commercial software)? This metric also focuses on the intersection recognition process, and provides insight into the algorithm's ability to not miss true intersections (false negatives).

(c) **Accuracy of intersection classification:**

$$Accuracy_c = \frac{\#\text{ of correctly classified intersections}}{\#\text{ of correctly recognized intersections}}. \tag{6}$$

The metric *Accuracy: Classification* specifically evaluates the accuracy of the intersection classification process of our approach. This metric is not applicable for commercial software since no existing commercial software is able to classify types of intersections.

(d) **Mean Absolute Error (MAE) of the measured ASTM grain size number:**

$$MAE = \frac{\sum_{i=1}^{n} |y_i - x_i|}{n} \tag{7}$$

where n is the total number of test images, y_i is the measured ASTM grain size number of the i^{th} test image by the algorithm, x_i is the ground truth ASTM grain size number (recall Eq. 2) of the i^{th} test image by manual labeling. This metric focuses on evaluating the overall performance of the algorithm (both intersection recognition and classification processes).

(e) **Accuracy of the measured average grain size:**

$$Accuracy_{gs} = 1 - \frac{|\text{measured } Avg_{gs} - \text{actual } Avg_{gs}|}{\text{actual } Avg_{gs}} \tag{8}$$

where *measured* Avg_{gs} is the average grain size (in mm^2) measured by the algorithm (our approach or commercial soft-

ware), and *actual* Avg_{gs} is the ground truth average grain size (in mm^2) determined by manually operated intercept method. This metric also focuses on evaluating the overall performance of the algorithm.

Experimental results for our approach and commercial software [32,33] are summarized in Table 3 with regard to the aforementioned metrics. In this table, results of our algorithm are measured in the case of handling discontinuous grain boundaries using the extension option, since it is the recommended option in general (see Section 3.4 for discussion of other options).

For grain boundary extraction and intersection recognition processes, although the semi-automatic procedure that applies commercial software [32,33] achieves a high *Recall (Recognition)* of 97%, its *Precision (Recognition)* is relatively low (81%), which indicates that the procedure is prone to generate false positive intersections and overestimate the average grain size. This is due to the limitation of basic image processing techniques used in the commercial software when handling complex image and material microstructure conditions. For example, to the best of our knowledge all commercial software extracts grain boundary pixels using global thresholding or edge detection techniques, which are less accurate on microscope images under conditions of unbalanced background illumination (recall Section 2.3.1). (For our test input, however, the illumination was almost always fairly well balanced.) As a larger source of concern, to the best of our knowledge commercial software (including iCALIBUR Master) generally only uses morphological operations to remove isolated image noise and microstructural artifacts. However, it is challenging for morphological operations to identify and remove noise and artifacts that are attached to grain boundaries (Fig. 10(c)).

In contrast, our algorithm employs a novel procedure to handle complex image and material microstructure conditions by exploiting image processing and geometric techniques such as adaptive thresholding, topological skeletons, and skeleton/graph pruning (Fig. 10(b)). The effectiveness of our algorithm on the grain boundary extraction and intersection recognition process is quantified by metrics *Precision (Recognition)* and *Recall (Recognition)* (both are $> 99\%$).

For the intersection classification process, our algorithm is able to classify recognized intersections into regular, junction, and end intersections with 98% accuracy (*Accuracy: Classification*). In the computation of the topological skeleton and junction points, noise/artifacts attached to grain junction areas may cause the computed junction positions to slightly deviate from the their true position, leading to incorrect intersection recognition and/or classification (Fig. 9(b) red arrows). In our experiments, this "junction position deviation" situation is infrequent ($< 2\%$) and does not cause a noticeable effect on the final measurement of grain size numbers (refer to low values of MAE and individual errors).

The MAE of ATSM grain size number measured by our approach is 0.023, with errors for individual images ranging from 0 to 0.096. (Compare this with what the standards estimate is the precision of the intercept method itself, ± 0.25 [7–10].) In comparison, for commercial software, the MAE is 0.394, with errors for individual images ranging from 0.012 to 1.116. Therefore, considering the entire grain size measurement process, our approach does not only achieve an overall higher accuracy (MAE), but also a greater consistency (considerably lower error ranges and worst-case errors). Similarly, for the accuracy of estimating the average grain size/area (*Accuracy: Avg Grain Size*), our algorithm outperforms the commercial software (98% to 76%).

Table 3
Accuracy comparison between our approach and commercial software. Our approach has better performance with respect to all the metrics.

	Ours	Software [32,33]
Precision (Recognition)	>99%	81%
Recall (Recognition)	>99%	97%
Accuracy: Classification	98%	-
MAE: Grain Size Number	0.023	0.394
Accuracy: Avg Grain Size	98%	76%

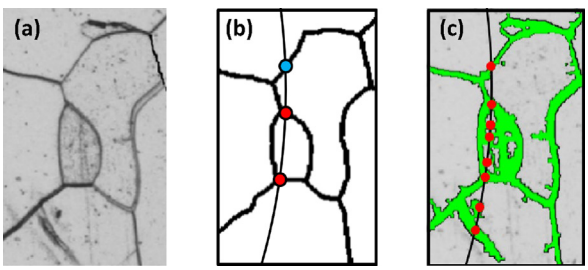

Fig. 10. Our algorithm outperforms commercial software on handling images with noise and/or microstructural artifacts: (a) an example input, (b) result using our algorithm, (c) result using commercial software [32,33], with a considerable number of false positive intersections.

3.3. Efficiency

The average measurement/computation time for different intercept method implementations (average per test microscope image) are listed in Table 4. Our automatic approach is orders of magnitude faster than manual operation and the commercial software approach. Note that in our experiments, manual operation and the semi-automatic commercial software approach are operated by experienced experts. For researchers who are not sophisticated in the intercept method and/or basic image processing techniques, the measurement time of manual operation and/or the commercial software approach would likely be even longer.

3.4. Handling discontinuous boundaries

Table 5 details the performance of our algorithm under different options for handling discontinuous grain boundaries. All three options are able to support our approach to automate the intercept method for a more accurate and efficient grain size measurement (compared to existing commercial software). Since the MAE and the computation time of the three options are similar, as discussed in Section 2.3.2, the extension option will generally be the best choice because it is the only option that is both fully automatic and is able to separate individual grains.

3.5. Additional grain size characterization capabilities

While implementing our algorithm with the extension or the manual connection option, the capability of individual grain separation enables our algorithm to both provide additional grain size and morphology information, as well as automate other standard test methods beyond the intercept method.

Table 4
Average measurement/computation time for different intercept method implementations (per test microscope image).

Manual	Our Approach	Software [32,33]
102.83s	5.03s	25.32s

Table 5
The mean absolute error (MAE) and efficiency (average computation time) of our algorithm under different options for handling discontinuous grain boundaries.

	MAE	Time
Extension	0.023	5.03s
Manual Connection	0.021	10.54s
Preservation	0.028	4.42s

3.5.1. Grain size statistics

Since individual grains are identified during our algorithm, the statistics of their size and morphology characteristics, such as area, aspect ratio, and orientation, can be automatically summarized as histograms (Fig. 11) for further microstructure analysis.

3.5.2. Automating other standard test methods

The accurate individual grain identification process enables our algorithm to automate not only the intercept method, but also other standard test methods for determining the average grain size of metallic materials, such as the planimetric method and the whole grain area method.

For the planimetric and the whole grain area method, according to standards ASTM E112 [7] and E1382 [24], identified grains are classified into one of three groups: (1) inside grains: grains that completely stay within the image region; (2) side grains: grains that intersect with the side(s) of the image, but do not intersect with image corners; (3) corner grains: grains that intersect with image corners. We classify our recognized grains accordingly (by examining if their interiors contain image boundary/corner pixels).

The planimetric method [7] measures the number of grains per unit area by considering the entire image region and counting the inside grains, side grains, and corner grains as 1, 0.5, and 0.25 effective grains respectively. In contrast, the whole grain area method [24] measures the average grain area by only considering the inside grains and their corresponding regions.

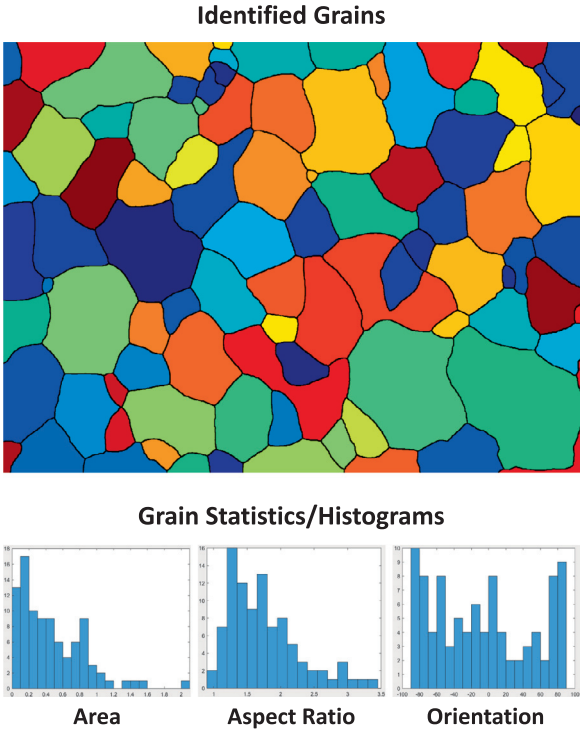

Fig. 11. Individual grains identified by our algorithm, and their statistics: histograms of grain areas, aspect ratios, and orientations.

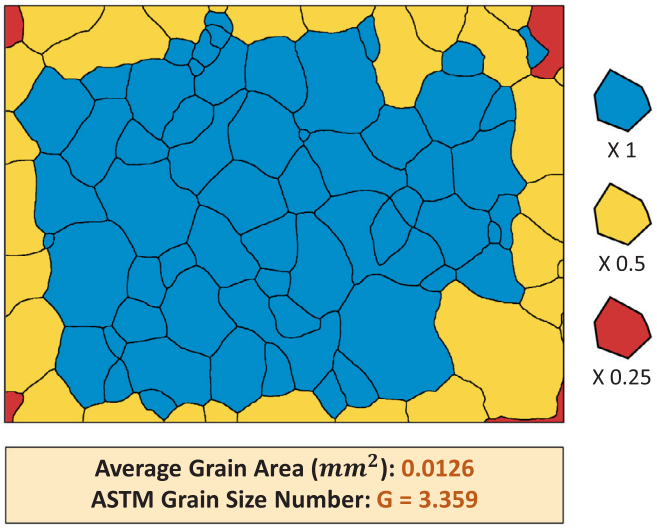

Fig. 12. Sample results of the extension of our algorithm to automate the planimetric method [7], where the inside grains, side grains, and corner grains are counted as 1, 0.5, and 0.25 effective grains respectively.

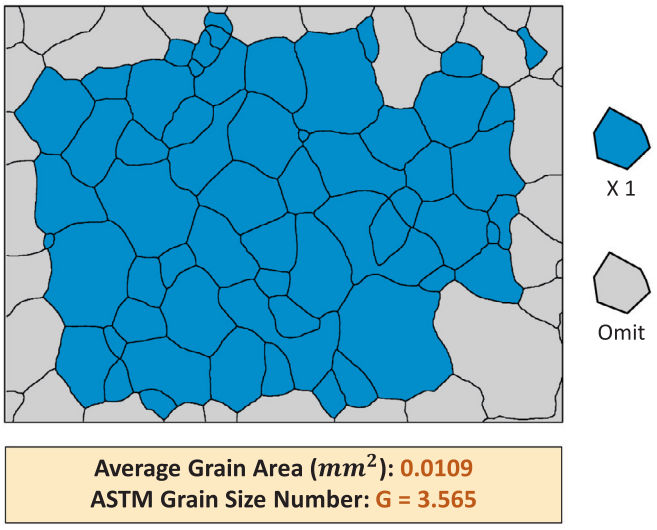

Fig. 13. Sample results of the extension of our algorithm to automate the whole grain area method [24], where only the inside grains (and their corresponding regions) are considered.

Example results of applying our algorithm's approach to handling and automating the planimetric method and the whole grain area method are illustrated in Fig. 12 and 13.

4. Limitations and future work

Although most image noise and microstructural artifacts can be removed in the image pre-processing and skeleton pruning processes, our algorithm may falsely identify large areas of stains or long scratches (Fig. 14(a)) as grain boundaries, which would cause an over-segmentation of grain structures and thus an underestimation of the average grain size.

Since metallographic images with large areas of microstructural artifacts are prone to affect the quality of both automatic and manual grain size measurement procedures, we suggest designing

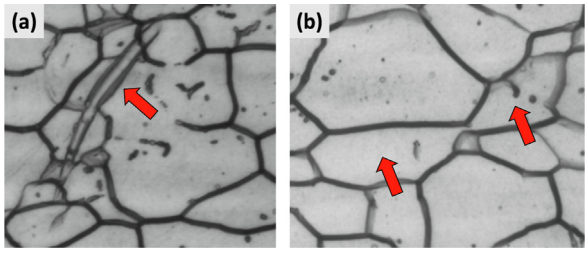

Fig. 14. Possible failure cases: (a) large scratches, which can lead to oversegmentation of grains; (b) a highly non-convex grain structure (red arrows pointing out its two halves that should potentially have been divided into two different grains, depending upon crystal orientation.

additional steps to recognize and eliminate such images prior to the measurement procedures. Potential solutions include implementing additional manual inspection, and/or designing machine learning models [34] for automatic detection of such artifacts.

Another interesting topic is the choice of how to handle highly non-convex grain structures. In the manual labeling process, since the overwhelming majority of individual grains are convex or nearly convex (e.g. regular equiaxed and elongated grains), researchers tend to segment highly non-convex grain structures into multiple convex (sub-) grain areas regardless of the absence of visible grain boundaries between these sub-areas. An example is shown in Fig. 14(b), where the highly non-convex grain would likely be labeled as two convex grains (red arrows) by metallurgical technicians, although no visible boundaries exist between them. Such highly non-convex grains could potentially be identified and highlighted when calculating grain size statistics (Section 3.5.1), allowing users to choose whether to further segment them or not.

5. Conclusion

In this paper, we have presented a novel algorithm to automate the intercept method for measuring the average grain size of metallic materials. By exploiting topological skeletons, our algorithm is able to extract continuous and closed grain boundaries, and measure the average grain size by recognizing and classifying intersections between selected test patterns and grain boundaries. To the best of our knowledge, this is the first automatic implementation of the intercept method that classifies and counts different types of intersections in compliance with international standards.

Due to the effectiveness of individual grain identification, our algorithm has not only been applied in the automation of the intercept method, but also been extended to automate other standard test methods such as the planimetric method and the whole grain area method. Our algorithm is also able to summarize grain statistics such as grain areas, aspect ratios, and orientations.

Our algorithm successfully automates and implements the intercept method, as validated on 200 real-world test microscope images (of different material microstructures under different specimen preparation conditions), achieving a robust overall accuracy ($> 98\%$) on the intersection recognition and classification processes. Compared to existing commercial software, our algorithm reduces the average measurement error 94%, from 0.394 to 0.023 grain size units, while reducing the average computation time by 80% (and 95% compared to manual calculation).

6. Data availability

Data will be made available on request.

Declaration of Competing Interest

The authors declare that they have no known competing financial interests or personal relationships that could have appeared to influence the work reported in this paper.

Acknowledgments

We gratefully acknowledge metallurgical technicians from Tsinghua University, University of Science and Technology Beijing, and China Iron and Steel Research Institute Group for preparing the samples and labeling the 200 test metallographic images.

References

[1] E.O. Hall, The deformation and ageing of mild steel: III Discussion of results, Proc. Phys. Soc. London, Sect. B 64 (9) (1951) 747.
[2] N.J. Petch, The cleavage strength of polycrystals, J. Iron Steel Inst. 174 (1953) 25–28.
[3] L. Tian, R. Zheng, C. Yuan, G. Yang, C. Shi, B. Zhang, Z. Zhang, Effect of grain size on the corrosion behavior of fully recrystallized ultra-fine grained 316L stainless steel fabricated by high-energy ball milling and hot isostatic pressing sintering, Mater. Charact. 174 (2021) 110995, https://doi.org/10.1016/j.matchar.2021.110995.
[4] A. Sarkar, M. Prasad, S.N. Murty, Effect of initial grain size on hot deformation behaviour of Cu-Cr-Zr-Ti alloy, Mater. Charact. 160 (2020) 110112, https://doi.org/10.1016/j.matchar.2019.110112.
[5] Q. Zhu, C. Wang, H. Qin, G. Chen, P. Zhang, Effect of the grain size on the microtensile deformation and fracture behaviors of a nickel-based superalloy via EBSD and in-situ synchrotron radiation X-ray tomography, Mater. Charact. 156 (2019) 109875, https://doi.org/10.1016/j.matchar.2019.109875.
[6] J. Shao, G. Yu, X. He, S. Li, R. Chen, Y. Zhao, Grain size evolution under different cooling rate in laser additive manufacturing of superalloy, Optics & Laser Technology 119 (2019) 105662, https://doi.org/10.1016/j.optlastec.2019.105662.
[7] ASTM E112-13(2021) Standard test methods for determining average grain size, Standard, ASTM International (2021). URL https://www.astm.org/e0112-13r21.html
[8] ISO 643:2019 Steels - Micrographic determination of the apparent grain size, Standard, International Organization for Standardization (2019). URL https://www.iso.org/standard/72193.html
[9] JIS G 0551:2020 Steels - Micrographic determination of the apparent grain size, Standard, Japanese Standards Association (2020).
[10] GB/T 6394-2017 Determination of estimating the average grain size of metal, Standard, Standardization Administration of China (2017).
[11] Y. Wang, G. Cheng, Quantitative evaluation of pit sizes for high strength steel: Electrochemical noise, 3-D measurement, and image-recognition-based statistical analysis, Materials & Design 94 (2016) 176–185, https://doi.org/10.1016/j.matdes.2016.01.016.
[12] J. Zhu, R. Balieu, X. Lu, N. Kringos, Microstructure evaluation of polymer-modified bitumen by image analysis using two-dimensional fast Fourier transform, Materials & design 137 (2018) 164–175, https://doi.org/10.1016/j.matdes.2017.10.023.
[13] X. Li, S. Shonkwiler, S. McMains, Fiber recognition in composite materials, in: 2021 IEEE International Conference on Image Processing (ICIP), IEEE, 2021, pp. 2623–2627.
[14] A. Campbell, P. Murray, E. Yakushina, S. Marshall, W. Ion, New methods for automatic quantification of microstructural features using digital image processing, Materials & Design 141 (2018) 395–406, https://doi.org/10.1016/j.matdes.2017.12.049.
[15] X. Li, S. Shonkwiler, S. McMains, Detection of resin-rich areas for statistical analysis of fiber-reinforced polymer composites, Composites Part B: Engineering 225 (2021) 109252, https://doi.org/10.1016/j.compositesb.2021.109252.
[16] H. Peregrina-Barreto, I. Terol-Villalobos, J. Rangel-Magdaleno, A. Herrera-Navarro, L. Morales-Hernández, F. Manríquez-Guerrero, Automatic grain size determination in microstructures using image processing, Measurement 46 (1) (2013) 249–258, https://doi.org/10.1016/j.measurement.2012.06.012.
[17] C.A. Paredes-Orta, J.D. Mendiola-Santibañez, F. Manriquez-Guerrero, I.R. Terol-Villalobos, Method for grain size determination in carbon steels based on the ultimate opening, Measurement 133 (2019) 193–207, https://doi.org/10.1016/j.measurement.2018.09.068.
[18] S. Banerjee, P.C. Chakraborti, S.K. Saha, An automated methodology for grain segmentation and grain size measurement from optical micrographs, Measurement 140 (2019) 142–150, https://doi.org/10.1016/j.measurement.2019.03.046.
[19] V. García-García, I. Mejía, F. Reyes-Calderón, Quantitative metallographic characterization of welding microstructures in Ti-containing TWIP steel by means of image processing analysis, Mater. Charact. 147 (2019) 1–10, https://doi.org/10.1016/j.matchar.2018.10.012.

[20] B. Flipon, V. Grand, B. Murgas, A. Gaillac, A. Nicolaÿ, N. Bozzolo, M. Bernacki, Grain size characterization in metallic alloys using different microscopy and post-processing techniques, Mater. Charact. 174 (2021) 110977, https://doi.org/10.1016/j.matchar.2021.110977.
[21] K. Gajalakshmi, S. Palanivel, N. Nalini, S. Saravanan, K. Raghukandan, Grain size measurement in optical microstructure using support vector regression, Optik 138 (2017) 320–327, https://doi.org/10.1016/j.ijleo.2017.03.052.
[22] M. Li, D. Chen, S. Liu, F. Liu, Grain boundary detection and second phase segmentation based on multi-task learning and generative adversarial network, Measurement 162 (2020) 107857, https://doi.org/10.1016/j.measurement.2020.107857.
[23] T.-C. Lee, R.L. Kashyap, C.-N. Chu, Building skeleton models via 3-D medial surface axis thinning algorithms, CVGIP: Graphical Models and Image Processing 56 (6) (1994) 462–478, https://doi.org/10.1006/cgip.1994.1042.
[24] ASTM E1382-97(2015) Standard test methods for determining average grain size using semiautomatic and automatic image analysis, Standard, ASTM International (2016). URL https://www.astm.org/e1382-97r15.html
[25] ASTM E3-11(2017) Standard guide for preparation of metallographic specimens, Standard, ASTM International (2017). URL https://www.astm.org/e0003-11r17.html
[26] E. Heyn, Short reports from the metallurgical and metallographical laboratory of the Royal Mechanical and Technical Testing Institute of Charlottenburg, The Metallographist 5 (1903) 39–64.
[27] H. Abrams, Grain size measurement by the intercept method, Metallography 4 (1) (1971) 59–78, https://doi.org/10.1016/0026-0800(71)90005-X.
[28] J.E. Hilliard, Estimating grain size by the intercept method, Metal Progress 85 (5) (1964) 99–102.
[29] N. Otsu, A threshold selection method from gray-level histograms, IEEE Transactions on Systems, Man, and Cybernetics 9 (1) (1979) 62–66.
[30] D. Bradley, G. Roth, Adaptive thresholding using the integral image, Journal of Graphics Tools 12 (2) (2007) 13–21, https://doi.org/10.1080/2151237X.2007.10129236.
[31] R.M. Haralick, L.G. Shapiro, Computer and robot vision, Vol. 1, Addison-Wesley, Reading, 1992.
[32] Leica Microsystems CMS GmbH, Leica Image Analysis Software (Version 1.4.6.110), Accessed: 2022-04-03. URL https://www.leica-microsystems.com/
[33] iCALIBUR R&D Center, iCALIBUR Master (Version 19.7.9.1), Accessed: 2022-03-12. URL https://www.sience-opt.com
[34] A. Chowdhury, E. Kautz, B. Yener, D. Lewis, Image driven machine learning methods for microstructure recognition, Comput. Mater. Sci. 123 (2016) 176–187, https://doi.org/10.1016/j.commatsci.2016.05.034.